# MULTISLICE MODEL OF ELECTRON BUNCH FOR STUDY OF BALLISTIC BUNCHING OF LOW EMITTANCE BEAMS

*A.M. Opanasenko[1], V.A. Goryashko[2]*
*[1]National Science Center "Kharkov Institute of Physics and Technology", Kharkov, Ukraine;*
*[2]Uppsala University, Sweden*
*E-mail: opanasenko@kipt.kharkov.ua*

At ballistic bunching of an electron beam the transverse distribution of space-charge field varies along a bunch greatly. It can lead to emittance growth unless to provide its compensation. To study this problem, a multislice model of a bunch of relativistic charged particles that needs no smallness of energy spread between slices are developed. This removes the limit on the value of the RF field that modulates the slices by velocity before their injection into a drift space. The longitudinal dynamics of each slice is determined by its interaction with the field of the entire bunch averaged over the slice. Transverse beam characteristics are found from a differential equation for root-mean-square envelope of a beam.

PACS: 29.20.Ej, 84.40.-x

## INTRODUCTION

One of the key problems of the modern rf electron accelerators is the bunching of intense beams into a sequence of ultra short bunches (from a few picoseconds to hundred of femtoseconds) with an rms normalized emittance close to the thermal level. For now the laser driven photoelectron emission is the most promising way of obtaining short (picoseconds) electronic bunches with charge about of 1 nC and a normalized transverse emittance less than 1 mm·mrad. This method is used in a number of accelerators in XFEL [1 - 3].

However, a short photocathode lifetime [4], and the need for ultra high vacuum (up to $10^{-11}$ Torr) as well high average power of a laser makes this technology also rather complicated for a small facility. Replacement of a photocathode by thermionic one will further reduce costs and make the electron gun even easier to operate.

Therefore, development of bunching methods of electron beams obtained from thermo-emission sources, that are distinguished by a long life time, up to 20000 or more hours [5], is still relevant. Opportunities of ballistic bunching of beams emitted from the DC thermolectronic gun and its subsequent longitudinal compression by magnetic compressors is demonstrated in the rf linac for the SACLA X-ray FEL (SPring-8 Angstrom Compact Free Electronic LAser, Japan) [6].

In the design of a rf accelerator for a combined photonic source of THz radiation based on a free-electron laser and Compton scattering [7, 8], it was shown that bunches with the charge of about 1 nC and the initial duration of 1 ns can be compressed longitudinally to several picoseconds under ballistic bunching. However, the Compton radiation source requires beams with an rms normalized emittance of about 1 mm·mrad in order of magnitude. Therefore, a bunching method should ensure both efficiency of bunch compression and to save the normalized beam emittance, or as much as possible slow down its growth.

Among the factors limiting achievement of the minimal bunch length is the initial energy spread of the beam and space charge fields. The most important reason that leads to growth of the effective transverse emittance is transverse space-charge (SC) forces linear on radius but inhomogeneous along a bunch.

In the paper [9], the first time the mechanism of the transverse normalized emittance growth caused by the SC field in short bunches was analyzed as well the method that compensates it proposed.

The authors of Ref. [10] for calculating influence of the SC field on dynamics of electron bunches accelerated in the LCLS (Linac Coherent Light Source) photoinjector developed the multi-slice model of an electron bunch. This approach is based on an assumption that each bunch is represented as a homogeneous cylinder whose length and radius can self-consistently change, while maintaining an uniform charge distribution within the bunch. By slicing the bunch in an array of thin cylinders, each one subject to the local field, one obtains also the energy spread and the emittance degradation due to phase correlation of RF and SC effects. But this approach does not provide to bunch a beam essentially. However, during the ballistic bunching, the SC field of the beam changes substantially in the drift space, that can lead to emittance growth, unless the special method of compensation is used.

In our paper, in the multislice approach we consider possibilities both ununiform charge density along a bunch and its deep compression under ballistic bunching. The longitudinal dynamics of each slice is determined by its interaction with the SC field of the entire bunch averaged over the slice. Transverse beam characteristics are found from a differential equation for root-mean-square envelope of the beam.

## 1. MULTISLICE MODEL

### 1.1. TRANSVERSE DYNAMICS EQUATIONS

The first equations of root-mean-square (rms) transverse sizes of a continuous charged beam in a channel with periodic focusing were derived by Kapchinskiy and Vladimirskiy [11]. Later the equations were generalized by Lapostole [12] and Sacherer [13]. This approach was also presented in detail in the article [14], on which we will reference at deriving correspond equations further.

We consider an axial symmetric bunch as a sequence of very thin slices. Each slice with current index ($i$) is characterized by next physical values:

a) an rms radius, $\sigma_r^{(i)}$,

$$\sigma_r^{(i)} = \sqrt{\left\langle r^2 \right\rangle^{(i)}}\ ; \qquad (1)$$

б) a normalized rms emittance, $\varepsilon_{n,r}^{(i)}$ [15]

$$\varepsilon_{n,r}^{(i)} = \frac{\left\langle \gamma \right\rangle^{(i)}}{2c}\sqrt{\left\langle r^2 \right\rangle^{(i)}\left\langle \dot{r}^2 \right\rangle^{(i)} - \left[\left\langle r\dot{r} \right\rangle^{(i)}\right]^2}\ ; \qquad (2)$$

c) a relativistic factor averaged over a slice, $\left\langle \gamma \right\rangle^{(i)}$, where $r$ and $\dot{r} = dr/dt$ are the radial coordinate and velocity. It is supposed that energy spread within each bunch is very small that it can be neglected.

Taking into account Eqs. (1) and (2), one can derive the differential equation for the rms radius of a slice in the paraxial approximation

$$\ddot{\sigma}_r^{(i)} + \frac{\dot{\gamma}_i}{\gamma_i}\dot{\sigma}_r^{(i)} + \left(\frac{eB_z(0,z_i)}{2m\gamma_i}\right)^2 \sigma_r^{(i)} = \frac{\left\langle rF_r^{(SC)} \right\rangle}{\sigma_r^{(i)} m\gamma_i} + \frac{\left(2\varepsilon_{n,r}^{(i)} c\right)^2}{\sigma_r^{(i)3}\gamma_i^2}, \qquad (3)$$

where $B_z(0,z)$ is the longitudinal magnetic field on the axis of a focusing solenoid, $F_r^{(SC)}$ is the radial component of the SC force.

### 1.2. SPACE CHARGE FORCE

Lorenz transverse force acting on the $i^{\text{th}}$ slice having the longitudinal coordinate $z_i$ is given as

$$\vec{F}_\perp^{(SC)}(r,z_i,t) = \\ = e\sum_j \left[\delta\vec{E}_\perp^{(j)}(r,z_i,t) + \vec{v}_z^{(i)} \times \delta\vec{B}_\perp^{(j)}(r,z_i,t)\right], \qquad (4)$$

where $\vec{v}_z^{(i)}$ is the average velocity of the $i^{\text{th}}$ slice; $\delta\vec{E}^{(j)}(r,z,t)$, $\delta\vec{B}^{(j)}(r,z,t)$ is the electric and magnetic space charge fields generated by the $j^{th}$ slice.

In order to find the fields from the $j^{th}$ slice, it is convenient to go into the rest frame of its slice $K'_j$ (as it is shown in Fig. 1) and then, finding the space charge electric field $E_\perp'^{(j)}(r',z')$, to came back to the laboratory system again:

$$\vec{F}_r^{(SC)}(r,z_i,t) = e\sum_j \left(1 - \frac{v_z^{(i)}v_z^{(j)}}{c^2}\right)\delta\vec{E}_r^{(j)}(r,z_i,t). \qquad (5)$$

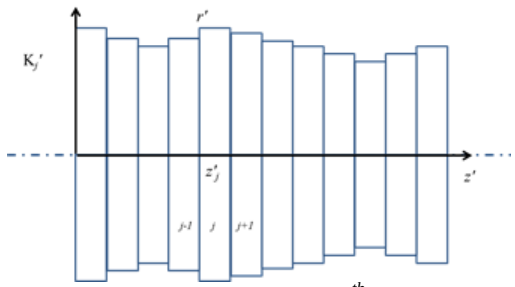


*Fig. 1. The rest frame of the $j^{th}$ slice, $K'_j$*

### 1.3. TRANSVERSE SPACE CHARGE FIELD

The radial component of the SC field in the laboratory system can be obtained from the Gauss law in the paraxial approximation, as

$$E_r(r,z,t) = \frac{r}{2}\frac{\rho(0,z,t)}{\varepsilon_0} - \frac{r}{2}\frac{\partial}{\partial z}E_z(0,z,t), \qquad (6)$$

where $\rho(0,z,t)$ is the charge density on a beam axis.

Then we find the SC electric field on the beam axis by going to the rest frame of the $j^{th}$ slice, $K'_j$. Consider the longitudinal electric field of a thin charged disc on its axis, as it is shown in Fig. 2.

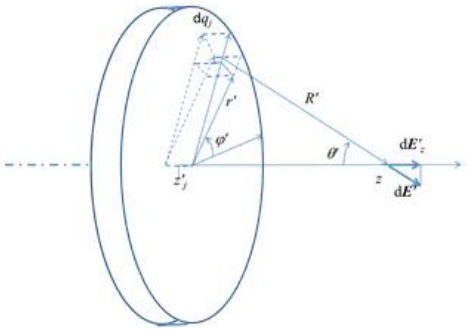


*Fig. 2. The longitudinal SC electric field of the $j^{the}$ disc on the axis in the rest frame, $K'_j$*

According to the Coulomb law, as it shown in Fig. 2, the electric field of the charged disc is given as

$$\delta E_z'^{(j)}(0,z') = sign\left(z' - z'_j\right) \\ \times \frac{\rho'(0,z'_j)\delta z'_j}{2\varepsilon_0}\left(1 - \frac{\left|z' - z'_j\right|}{\sqrt{r_j'^2 + \left(z' - z'_j\right)^2}}\right), \qquad (7)$$

where $\rho'(0,z'_j)$ is the charge density on beam axis in the $K'_j$ frame.

Performing the Lorentz transformation in Eq. (7), the longitudinal electric field on the beam axis in the laboratory frame is obtained as superposition of the fields from the each slice. Then using Eqs. (6) and (5) we find the transverse component of the SC field acting on the $i^{th}$ slice in the paraxial approximation, as

$$F_r^{(SC)}(r,z_i,t) = e\frac{r}{2}\sum_j \left(1 - \frac{v_z^{(i)}v_z^{(j)}}{c^2}\right)\times \\ \frac{\rho(0,z_j,t)\delta z_j}{2\varepsilon_0}\frac{\left(\frac{r_j}{\gamma_j}\right)^2}{\left(\sqrt{\left(\frac{r_j}{\gamma_j}\right)^2 + \left(z_i - z_j\right)^2}\right)^3}. \qquad (8)$$

### 1.4. EQUATIONS OF LONGITUDINAL MOTION

In order to close the self-consistent system we have to derive the equation of longitudinal dynamics of slices

$$\frac{dp_z^{(i)}}{dt} = e\overline{E_z^{(SC)}}(z_i,t), \qquad (9)$$

where $p_z^{(i)}$ is the longitudinal momentum of the $i^{\text{th}}$ slice, $\overline{E_z^{(SC)}}(z_i,t)$ is the longitudinal component of the SC electric field averaged over the $i^{\text{th}}$ slice as

$$\overline{E_z^{(SC)}}(z_i,t) = \frac{1}{\pi r_i^2}\int_0^{2\pi}\int_0^{r_i} E_z^{(SC)}(r,\varphi,z_i,t)\,r\,dr\,d\varphi\ . \qquad (10)$$

By transiting into the rest frame of the $j^{th}$ slice $K'_j$ and solving Poisson's equation by the method given in


ISSN 1562-6016. ВАНТ. 2018. №3(115)

Ref. [16] (see the chapter 12) we can express the SC potential through the Fourier integral

$$\Phi'\left(r', r'_j, z'-z'_j\right) = \int_0^\infty e^{-k\left|z'-z'_j\right|} J_0\left(kr'\right) B_0\left(r'_j, z'_j, k\right) dk, \quad (11)$$

where $B_0\left(r'_j, z'_j, k\right)$ is the unknown function determined through the boundary conditions for the electric field at $z' = z'_j$

$$B_0\left(r'_j, z'_j, k\right) = \lim_{z'\to z'_j} sign\left(z'-z'_j\right) \times \frac{\rho'\left(0, z'_j\right)\delta z'_j}{2\varepsilon_0} r'_j \frac{J_1\left(kr'_j\right)}{k}. \quad (12)$$

Substituting the last into Eq.(11), and differencing per $z'$, we find the longitudinal component of SC electric field of the $j^{th}$ slice in the integral form

$$\delta E_z'^{(j)}\left(r', r'_j, z'-z'_j\right) = sign\left(z'-z'_j\right) \times \frac{\rho'\left(0, z'_j\right)\delta z'_j}{2\varepsilon_0} r'_j \int_0^\infty e^{-k\left|z'-z'_j\right|} J_0\left(kr'\right) J_1\left(kr'_j\right) dk. \quad (13)$$

Radial profiles of the longitudinal component of the SC field from the $j^{th}$ slice normalized to the field at the slice surface $\delta E_0'^{(j)} = sign\left(z'-z'_j\right)\frac{\rho'\left(0, z'_j\right)\delta z'_j}{2\varepsilon_0}$ are shown in Fig. 3. The radial profiles are built at different distances $Z' = \left|z'-z'_j\right|/r'_j$ from the $j^{th}$ slice. One can see that $\delta E_z'^{(j)}\left(r', r'_j, z'-z'_j\right)$ is independent from the radius $r'$ on the surface of the $j^{th}$ slice ($Z' = 0$) and equals the surface charge density. Apart too this Fig. 3 shows that the field ceases to be independent on the radius $r'$ far from the slice $Z' \geq 5$.

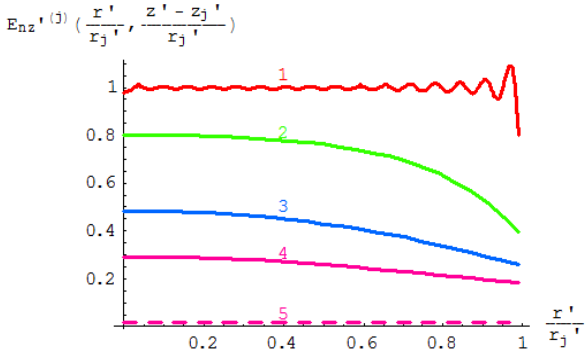


*Fig. 3. Radial profiles of the z-component of the SC field from the $j^{th}$ slice normalized to the field at the slice surface taken at different relative distances $Z' = \left|z'-z'_j\right|/r'_j$ from the slice. The curves with numbers 1, 2, 3, 4, 5 correspond to Z'=0, 0.2, 0.6, 1, 5, accordingly*

Next, by averaging the field of the $j^{th}$ slice Eq. (13) over the disc with the radius $r'$, one can obtain as

$$\overline{\delta E_z'^{(j)}}\left(r', r'_j, z'-z'_j\right) = sign\left(z'-z'_j\right) \times \frac{\rho'\left(0, z'_j\right)\delta z'_j}{2\varepsilon_0} \frac{2r'_j}{r'} \int_0^\infty dk e^{-k\left|z'-z'_j\right|} J_1\left(kr'_j\right) \frac{J_1\left(kr'\right)}{k}, \quad (14)$$

which is normalized by $\delta E_0'^{(j)}$ shown along $Z'$ in Fig. 4 for two relative radiuses $R' = r'/r'_j$.

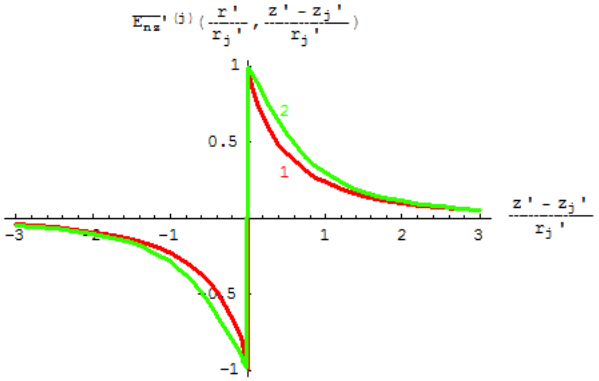


*Fig. 4. The longitudinal distributions of the averaged and normalized SC field Eq. (14) for two relative radiuses $R' = r'/r'_j$. The curves 1, 2 correspond to $R'$ =1, 0.01, accordingly*

### 1.5. ANALYTICAL APPROXIMATION

From Fig. 4 one can see that within relative distances $0 < \left|z'-z'_j\right|/r'_j < 2$ the field on the axis is different from the field averaged over the slice. Let us find the analytical approximation of the difference

$$\Delta\overline{E_{nz}'^{(j)}} = \frac{\overline{\delta E_z'^{(j)}}\left(0, r'_j, z'-z'_j\right) - \overline{\delta E_z'^{(j)}}\left(r', r'_j, z'-z'_j\right)}{\delta E_0'^{(j)}}.$$

For this Eq. (14) can be represented as

$$\overline{\delta E_z'^{(j)}}\left(r', r'_j, z'-z'_j\right) = sign\left(z'-z'_j\right) \times \frac{\rho\left(0, z'_j\right)\delta z'_j}{2\varepsilon_0}\left(1 - \frac{\left|z'-z'_j\right|/r'_j}{\sqrt{1+\frac{\left(z'-z'_j\right)^2}{r_j'^2}}} - \Delta\overline{E_{nz}'^{(j)}}\right), \quad (15)$$

where the difference $\Delta\overline{E_{nz}'^{(j)}}$ is determined as:

$$\Delta\overline{E_{nz}'^{(j)}} = \int_0^\infty dx e^{-x\frac{\left|z'-z'_j\right|}{r'_j}} J_1(x)\left[1 - \frac{2J_1\left(xr'/r'_j\right)}{xr'/r'_j}\right]. \quad (16)$$

Further we expand a function in the square brackets of Eq. (16) into Taylor's series in degrees of $xr'/r'_j$ and build the following approximation

$$\Delta\overline{E_{nz}'^{(j)}} \approx \frac{3}{8}R'^2 \frac{\left|Z'\right|}{\left(1+Z'^2\right)^{\frac{5}{2}}} e^{-\frac{5}{24}R'^2\frac{\left(4Z'^2-3\right)}{\left(1+Z'^2\right)^2}}. \quad (17)$$

Coming back into the laboratory frame K, the longitudinal component of the SC field averaged over the slice is given as the superposition of the fields from each slice

$$\overline{E_z^{(SC)}}(r,z,t)=\sum_{j=1}^{N}\delta E_0^{(j)}\left[1-\frac{\gamma_j\frac{|z-z_j|}{r_j}}{\sqrt{1+\gamma_j^2\frac{(z-z_j)^2}{r_j^2}}}\right.$$
$$\left.-\frac{3}{8}\frac{r^2}{r_j^2}\frac{\gamma_j\frac{|z-z_j|}{r_j}}{\left(1+\gamma_j^2\frac{(z-z_j)^2}{r_j^2}\right)^{\frac{5}{2}}}e^{-\frac{5}{24}\frac{r^2}{r_j^2}\frac{\left(4\gamma_j^2\frac{(z-z_j)^2}{r_j^2}-3\right)}{\left(1+\gamma_j^2\frac{(z-z_j)^2}{r_j^2}\right)^2}}\right], \quad (18)$$

where $\delta E_0^{(j)}=sign(z-z_j)\frac{\rho(0,z_j)\delta z_j}{2\varepsilon_0}$.

## 2. SELF-CONSISTENT MODEL

Taking into account the equations obtained above, we can write the system of self-consistent equations of the motion of slices with the boundary conditions in the following form:

i) the equation for the rms radius of the $j^{th}$ slice

$$\ddot{\sigma}_r^{(i)}+\frac{\dot{\gamma}_i}{\gamma_i}\dot{\sigma}_r^{(i)}+\left(\frac{eB_z(0,z_i)}{2m\gamma_i}\right)^2\sigma_r^{(i)}=\frac{\sigma_r^{(i)}}{m\gamma_i}\frac{\partial}{\partial r}F_r^{(SC)}(r,z_i,t)+\frac{\left(2\varepsilon_{n,r}^{(i)}c\right)^2}{\sigma_r^{(i)3}\gamma_i^2}, \quad (19)$$

where

$$\frac{\partial}{\partial r}F_r^{(SC)}(r,z_i,t)=\frac{e}{4\pi\varepsilon_0}\frac{t_b}{N}\sum_{j=1}^{N}\left(1-\beta_z^{(i)}\beta_z^{(j)}\right)\times \quad (20)$$
$$\frac{I(0,t_{0j})}{\sigma_r^{(j)2}}\left(\frac{\sigma_r^{(j)}}{\gamma_j}\right)^2\left/\left(\sqrt{2\left(\frac{\sigma_r^{(j)}}{\gamma_j}\right)^2+(z_i-z_j)^2}\right)^3\right.;$$

ii) the equation of the longitudinal motion of the $j^{th}$ slice in the drift space

$$\dot{z}_i(t)=c\beta_z^{(i)}(t), \quad (21)$$

where

$$\dot{\beta}_z^{(i)}=\frac{e\overline{E_z^{(SC)}}(z_i,t)}{mc\gamma_i^3}=\frac{e}{4\pi\varepsilon_0 mc\gamma_i^3}\frac{t_b}{N}\times$$
$$\sum_{j=1}^{N}sign(z_i-z_j)\frac{I(0,t_{0j})}{\sigma_r^{(j)2}}\left[1-\frac{\gamma_j\frac{|z_i-z_j|}{\sqrt{2}\sigma_r^{(j)}}}{\sqrt{1+\gamma_j^2\frac{(z_i-z_j)^2}{2\sigma_r^{(j)2}}}}\right.$$
$$\left.-\frac{3}{8}\frac{\sigma_r^{(i)2}}{\sigma_r^{(j)2}}\frac{\gamma_j\frac{|z_i-z_j|}{\sqrt{2}\sigma_r^{(j)}}}{\left(1+\gamma_j^2\frac{(z_i-z_j)^2}{2\sigma_r^{(j)2}}\right)^{\frac{5}{2}}}e^{-\frac{5}{24}\frac{\sigma_r^{(i)2}}{\sigma_r^{(j)2}}\frac{\left(2\gamma_j^2\frac{(z_i-z_j)^2}{\sigma_r^{(j)2}}-3\right)}{\left(1+\gamma_j^2\frac{(z-z_j)^2}{2\sigma_r^{(j)2}}\right)^2}}\right] \quad (22)$$

iii) the boundary conditions:

$$t_{0i}=-\frac{t_b}{2}+(i-1)\frac{t_b}{N-1},\ i=1,2..N,$$
$$z_i(t_{0i})=0,\ \beta_z^{(i)}(t_{0i})=\beta_{z,0}^{(i)}, \quad (23)$$
$$\dot{\sigma}_r^{(i)}=\dot{\sigma}_{r,0}^{(i)},\ \sigma_r^{(i)}(t_{0i})=\sigma_{r,0}^{(i)},$$

where $t_b$ is the initial bunch duration, $N$ is a number of the slices in the bunch, $I(0,t_0)$ is the initial beam current.

## 3. RESULTS OF NUMERICAL SIMULATION OF BALLISTIC BUNCHING

The differential equations (19) - (23) were calculated by the Runge-Kuta method of the fourth order of accuracy. The electron beam at the entrance to the drift space was considered with the parameters given in the Table, which are characteristics of the project of the combined THz/X radiation source, on the basis of a free electrons lasing and Compton scattering [7, 8].

*Beam parameters*

| | |
|---|---|
| Initial beam current | 1 A |
| Initial beam duration | 1 ns |
| Beam energy | 400 keV |
| RMS normalized beam emittance | 0.4 mm·mrad |
| RMS beam radius | 2 mm |

The Figs. 7 and 8 depict the distributions of the longitudinal SC force averaged over of each slice and the radial SC force taken on the rms slice radius.

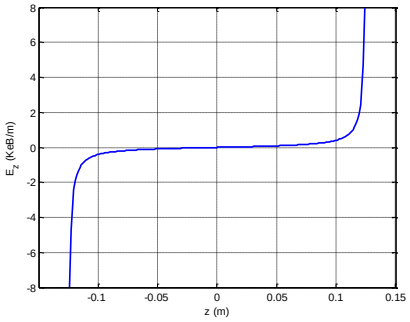


*Fig. 7. The distribution of the averaged longitudinal SC force along the bunch*

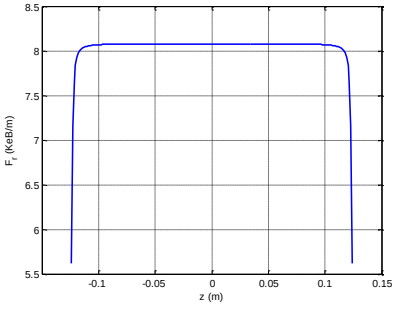


*Fig. 8. The distribution of the radial SC force along the bunch taken at the rms slice radius*

As it should expected, the SC field of a homogeneous long bunch is strongly variated only along the edges, which is a source of growth of the effective transverse emittance. In order to investigate how the longitudinal profile of the SC field will be transformed during ballistic bunching, consider the 400 keV beam that is premodulated by velocity by a field in RF cavities with fre-


ISSN 1562-6016. ВАНТ. 2018. №3(115)

quencies of 176.1 MHz and 528.3 MHz (the third harmonic), by a law

$$\beta_z(\tau_0) = \frac{\beta_{z,0}}{1 + A + B\tau_0 + C\tau_0^2 + D\tau_0^3}, \quad (24)$$

which approximates to the hyperbolic dependence of the initial velocity on the time of the flight of electrons at entrance to the drift space [7], for the parameters: $\beta_{z,0}$ = 0.828, $A$ = 0.00670805, $B$ = -0.0781966, $C$ = -0.00607415, $D$ = 0.0126568, where $\tau_0 = \omega t_0$.

### 3.1. KINEMATIC APPROXIMATION

If we do not take into account the influence of a SC field, so the bunch peak current under ballistic bunching, will change by a law

$$I(\varsigma, \tau_0) = \frac{I(0, \tau_0)}{1 + \varsigma \dfrac{d}{d\tau_0}\dfrac{1}{\beta_z(\tau_0)}}, \quad (25)$$

where $\varsigma = z\,\omega/c$ is the dimensionless longitudinal coordinate. The distance that the beam will pass to the point of the maximum compression is

$$\varsigma_f = \varsigma_0 - \frac{\beta_{z,0}}{B + 2C\tau_0 + 3D\tau_0^2}, \quad (26)$$

where $\varsigma_0$ is the deviation of a slice coordinate from the geometric center of the initial bunch that has the velocity $\beta_{z,0}$.

In Fig. 9 it is shown the histogram of the peak current distribution at the moment of the maximum bunching in the immediate vicinity of the cross section with the coordinate $\varsigma_f = 2.896\ m\,\omega/c$. The minimum width of the column of the histogram is 0.33 mm, which corresponds to the time span of 1.355 psec. From Fig. 9 it is seen that the width at the half-height is about 1.65 mm.

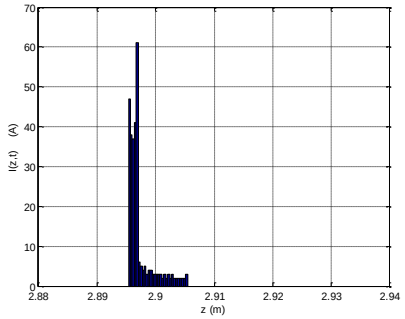


*Fig. 9. The distribution of a bunch peak current at time of the maximum compression*

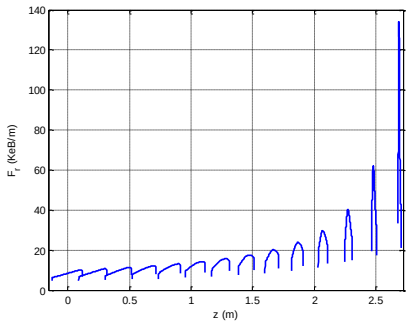


*Fig. 10. The longitudinal profiles of the radial SC force in the drift space at different moments of time*

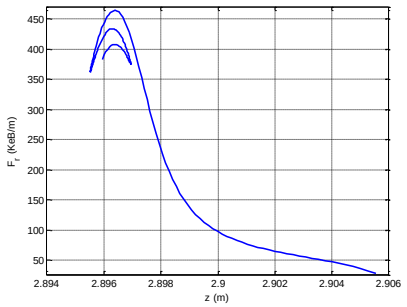


*Fig. 11. The longitudinal profiles of the radial SC force at the maximal compression*

In Figs. 10,11 it is depicted the longitudinal profiles of the radial component of the SC force along bunches compressing in the longitudinal direction in the drift space at different moments of time.

It should note that ambiguity of the radial component of the SC force in the region of the maximal bunching (see Fig. 11) is due to its dependence on an electron energy (as it can be seen from Eq. (8)). At the time of the maximum compression electrons with different energies can have the same longitudinal coordinate. This is clearly seen from the following figure (Fig. 12), which shows the dependence of the energy on the electron coordinate within the bunch at a moment of the maximum bunching.

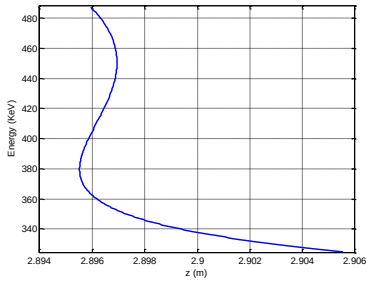


*Fig. 12. The distribution of electron energy along the bunch at the maximal compression*

### 3.2. SELF-CONSISTENT DYNAMICS

#### 3.2.1. CHOIS OF MAGNETIC FIELD OF SOLENOID

In order to minimize emittance growth a drifting beam, (at least in that part of the drift space where the bunch can be considered as long ($\gamma_0\sigma_z >> \sigma_r$)) it is necessary to fulfill conditions of the equilibrium Brillouin flow, for which the magnetic field of a solenoid satisfies an equation [17].

$$B_z(0, z) = C\,\mu_0 \frac{I_a}{2\pi\sigma_r}\sqrt{\frac{I(z)}{I_a\beta_0\gamma_0}}, \quad (27)$$

and the beam at the entrance to the drift space must have the minimal radial divergence. Here the factor $C \approx 1$ is a correction factor, which is determined by the finite beam length and must be set numerically; $I_a$ = 17045 A.

As a first step at optimization of the longitudinal profile of the magnetic field, on the one side, and in order to test the physical model, on the other side, calculations have been made that specify the magnitude of the magnetic field for the non-modulated beam. The results of such calculations are presented in Fig. 13, where the dependencies of the rms beam radius are shown for different values of the correction factor $C$.

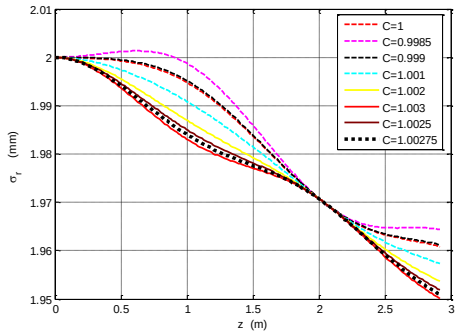


*Fig. 13. The rms beam radius v.s. longitudinal coordinates in the drift space at different values of the correction factor C*

From Fig. 13 it follows that the magnetic field Eq. (32) with the correction factor C = 1.00275 ($B_{z,0} = 108\ Гс$) maximally satisfices the condition of the equilibrium Brillouin flow at the beginning drift. In this case the evolution of the rms normalized transverse emittance that one can see in Fig. 14, oscillates at the start level that coincides well with the results obtained in Ref. [17].

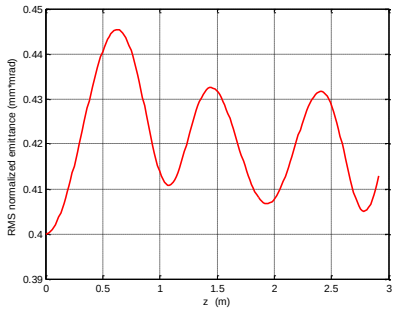


*Fig. 14. The evolution of the rms normalized transverse beam emittance in the drift space*

### 3.2.2. IMPACT OF SC FIELD ON BUNCHING

In this subsection we consider results of calculating ballistic bunching of the beam premodulated on velocity (see Eq. (24)), taking into account a self-consistent interaction with its own SC field. The distributions of the bunch peak current in the drift space at different moments of time are shown in Fig. 15. The minimum width of the column of the histogram is the same as in Fig. 9.

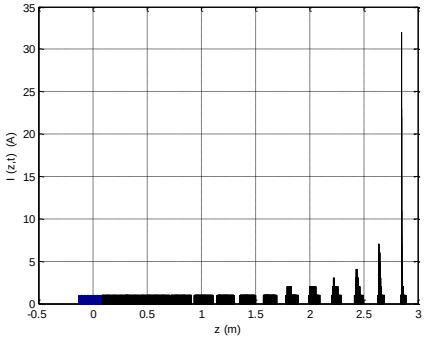


*Fig. 15. The distributions of the bunch peak current in the drift space at different moments of time*

In Fig. 16 one can see the image of the distribution of the bunch peak current at the time of the maximal compression.

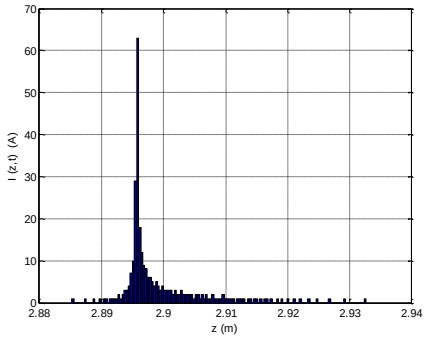


*Fig. 16. The distribution of the bunch peak current at the time of the maximal bunch compression*

It should note that despite the "tails" of the bunch significantly lengthened because of the fact that the longitudinal component of the SC field acts continuously during drift, as one can see from the comparison of Figs. 9 and 16, however, we can also observe as well the significant reduction of the bunch width at half-height from 1.65 mm (see Fig. 9) to 0.33 mm (see Fig. 16). As it expects, due to act of the longitudinal component of the SC field, there is no overtaking of the slices. This is clearly seen from the next figure, which shows as the slice energy dependence on z-coordinates within the bunch at the moment of the maximum longitudinal compression.

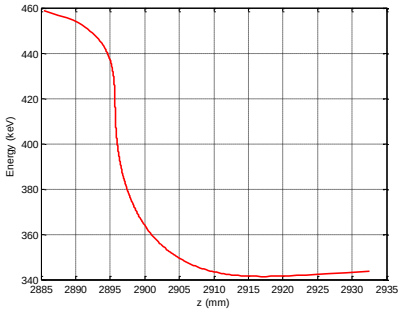


*Fig. 17. The distribution of an electron energy along the bunch at the maximal compression*

The unexpected 5-fold shortening of the bunch (see Fig. 16), as compared with the kinematic approximation (see Fig. 9), can be explained by the significant increase of the transverse size of the slices as it is seen from Fig. 18. This leads to decrease of the beam charge density in this area and, as a consequence, to reduce the longitudinal SC field of repulsion of the slices.

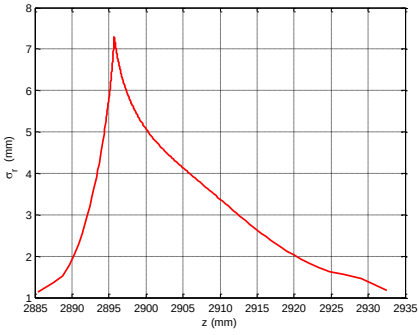


*Fig. 18. The distribution of the rms slice radius along the bunch at the maximal compression*

The transformations of the distribution of the SC forces at the moment of the maximum compression are shown in Figs. 19, 20.

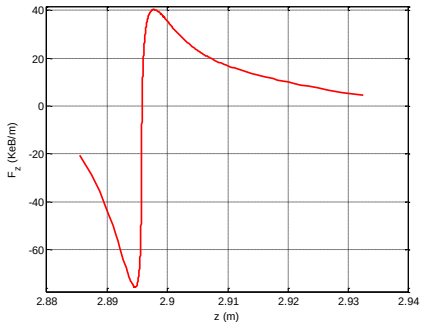


*Fig. 19. The distribution of the averaged longitudinal SC force along a bunch at the maximal compression*

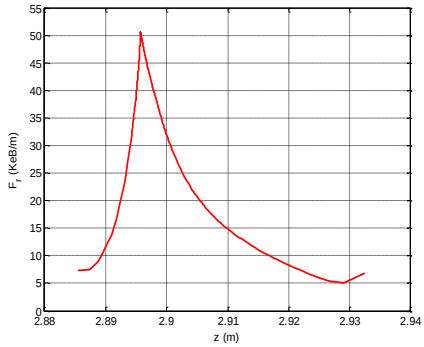


*Fig. 20. The longitudinal profiles of the radial SC force taken at the maximal compression*

The next Figs. 21, 22 demonstrate the evolution of such statistical beam parameters during the drift as: the rms radius and normalized transverse emittance.

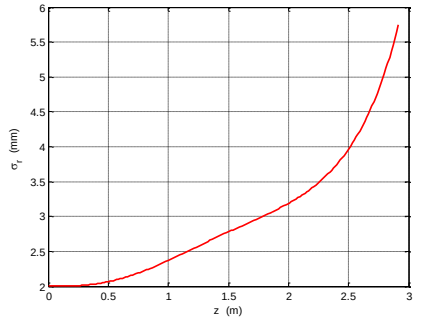


*Fig. 21. The rms beam radius in the drift space*

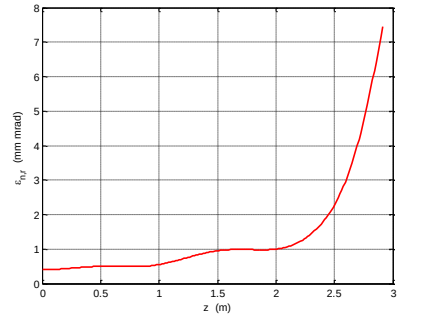


*Fig. 22. The rms normalized transverse beam emittance along the drift space*

The beam emittance growth, that is observed starting from the mark 2 *m* of the drift space (see Fig. 22), can be a consequence of two factors. On the one hand, from this place it begins to growth heterogeneity of the radial component of the SC field that results in non synchronous rotate of the slices on the phase plane ($\sigma'_r$, $\sigma_r$) and thus leads to increase of the effective emittance. On the other hand, from this mark the beam radius begins to increase, (see Fig. 21), that can cause as well growth of the correlated transverse emittance due to its connection with the longitudinal emittance [15]. The estimations show that the transverse normalized emittance, correlated with longitudinal one, increases as ~ $\sigma_r^4$. Therefore in order to switch off this mechanism of the emittance growth we have to optimize the longitudinal profile of the focusing magnetic field, so that the beam radius keeps the original value.

## SUMMARY

The multislice method of calculating interaction of an electron beam with own SC field was developed that, in contrast to the similar approaches proposed earlier, takes into account the possibility of realizing not only a bunch with uniform charge density, but also allows its deeply transformation in a drift space.

The developed approach does not require of smallness of inter-slice energy spread, avoiding restriction on a magnitude of RF field that modulates the beam on velocity, before it to be injected into a drift space.

The multislice method allows to calculate self-consistence dynamics under ballistic bunching and to study conditions of the maximal longitudinal compression of the bunch and factors that restrict their as well to optimize the longitudinal profile of an external magnetic field with aim to reach the minimal transverse normalized effective emittance.

This work was supported in part by Stockholm-Uppsala Centre for Free Electron Laser Research, and Swedish Research Council.

## REFERENCES

1. J. Andruszkow et al. First Observation of Self-Amplified Spontaneous Emission in a Free-Electron Laser at 109 nm Wavelength // *PRL*. 2000, v. 85, № 18, p. 3825-3829.
2. J. Arthur et al. Linac Coherent Light Source (LCLS) Conceptual Design Report // *SLAC-R-593*. April 2002, UC-414, 554 p.
3. The European X-Ray Free-Electron Laser. Technical design report // by editors Massimo Altarelli, et al. DESY 2006-097. July 2007, 630 p.
4. F. Sannibale et al. Status, plans and recent results from the APEX project at LBNL // *Proceedings of FEL2015*. 2015, Daejeon, Korea, p. 81-84.
5. K. Togaw et al. CeB6 electron gun for low-emittance injector // *Phys. Rev. STAB*. 2007, v. 10, p. 020703-10.
6. Tsumoru Shintake et al. Stable operation of a self-amplified spontaneous-emission free-electron laser in the extremely ultraviolet region // *Phys. Rev. STAB*. 2009, v. 12, p. 070701-12.
7. A. Opanasenko, V. Mytrochenko, P. Salen, V. Zhaunerchyk, V.A. Goryashko. Fundamental limits of ballistic bunching of high-brightness electron beams // *Proceedings of IPAC2014*. Dresden, Germany (MOPRO091), 2014, p. 304-306.
8. V.A. Goryashko, A. Opanasenko, V. Zhaunerchyk. A Swedish compact linac-based THz/X-ray source at FREIA // *Proceedings of FEL2014*. Basel, Switzerland TUP079, 2014, p. 545-548.

9. B.E. Carlsten. New photoelectric injector design for the Los Alamos National Laboratory XUV FEL accelerator // *NIM.* 1989, v. A 285, p. 313-319
10. M. Ferrario, J.E. Clendenin, D.T. Palmer, J.B. Rosenzweig, L. Serafini. HOMDYN Study for the LCLS RF Photo-Injector // *SLAC-PUB-8400*, March 2000, LCLS-TN-00-04, LNF-00/004, p. 1-31.
11. I.M. Kapchinskij and V.V. Vladimirskij. Limitations for proton beam current in a strong focusing linear accelerator associated with the beam space-charge // *Proc. Int. Conf. on High Energy Accelerators and Instrumentation.* CERN, 1959, p. 274.
12. P.M. Lapostole. Possible Emittance Increase Through Filamentation Due to Space Charge in continuous beams // *IEEE Trans. Nucl. Sci.* 1971, NS-18, p. 1101.
13. P. Sacherer. RMS Envelope Equations with space charge // *IEEE Trans. Nucl. Sci.* 1971, NS-18, p. 1105.
14. Massimo Ferrario. Accelerator physics: basic principles on beam focusing and transport // *SPARC-BD-12/01*. 2012, p. 1-23.
15. Klaus Floettmann. Some basic features of the beam emittance // *Phys. Rev. STAB.* 2003, v. 6, p. 034202-7.
16. Дж. Джексон. *Класична електродинаміка.* М.: "Мір", 1965, 702 с.(in Russian).
17. L. Serafini, J.B. Rosenzweig. Envelope analysis of intense relativistic quasilaminar beams in rf photoinjectors: A theory of emittance compensation // *Phys. Rev. E*. 1997, v. 55, № 6, p. 7565-7590.

*Article received 22.02.2018*

## МУЛЬТИДИСКОВАЯ МОДЕЛЬ ЭЛЕКТРОННОГО СГУСТКА ДЛЯ ИССЛЕДОВАНИЯ БАЛЛИСТИЧЕСКОГО ГРУППИРОВАНИЯ НИЗКОЭМИТАНСНЫХ ПУЧКОВ

***А.М. Опанасенко, В.А. Горяшко***

При баллистическом группировании электронного пучка неоднородность вдоль сгустка поперечной компоненты поля пространственного заряда существенно увеличивается, что может привести к росту поперечного эмитанса, если не будет задействован специальный способ его компенсации. Для исследования этой проблемы развита мультидисковая модель сгустка релятивистских заряженных частиц, не требующая условия малости междудискового энергетического разброса. Это снимает ограничения на величину поля, модулирующего пучок по скорости перед его инжекцией в дрейфовое пространство. Поперечные характеристики динамики сгустка мы находим из решения дифференциального уравнения для среднеквадратичного размера огибающей пучка.

## МУЛЬТИДИСКОВА МОДЕЛЬ ЕЛЕКТРОННОГО ЗГУСТКА ДЛЯ ДОСЛІДЖЕННЯ БАЛІСТИЧНОГО ГУРТУВАННЯ НИЗЬКОЕМІТАНСНИХ ПУЧКІВ

***А.М. Опанасенко, В.А. Горяшко***

При балістичному гуртуванні електронного пучка неоднорідність вздовж згустка поперечної компоненти поля просторового заряду суттєво збільшується, що може призвести до росту поперечного емітансу, якщо не буде задіяний спеціальний спосіб його компенсації. Для дослідження цієї проблеми розвинуто мультидискову модель згустка релятивістських заряджених частинок, яка не потребує умови малості між-дискового енергетичного розкиду. Це знімає обмеження на величину поля, що модулює пучок по швидкості, перед його інжекцією в дрейфовий простір. Поперечні характеристики динаміки згустка знаходимо із рішення диференційного рівняння для середньоквадратичного розміру огинаючої пучка.